# Appendix

In this work, we selected semi-regular, demi-regular, polygon monohedral, and Penrose aperiodic tessellation patterns to construct the microstructures of the two phases. The schematic diagrams of all the models and the results of the calculations are shown below.

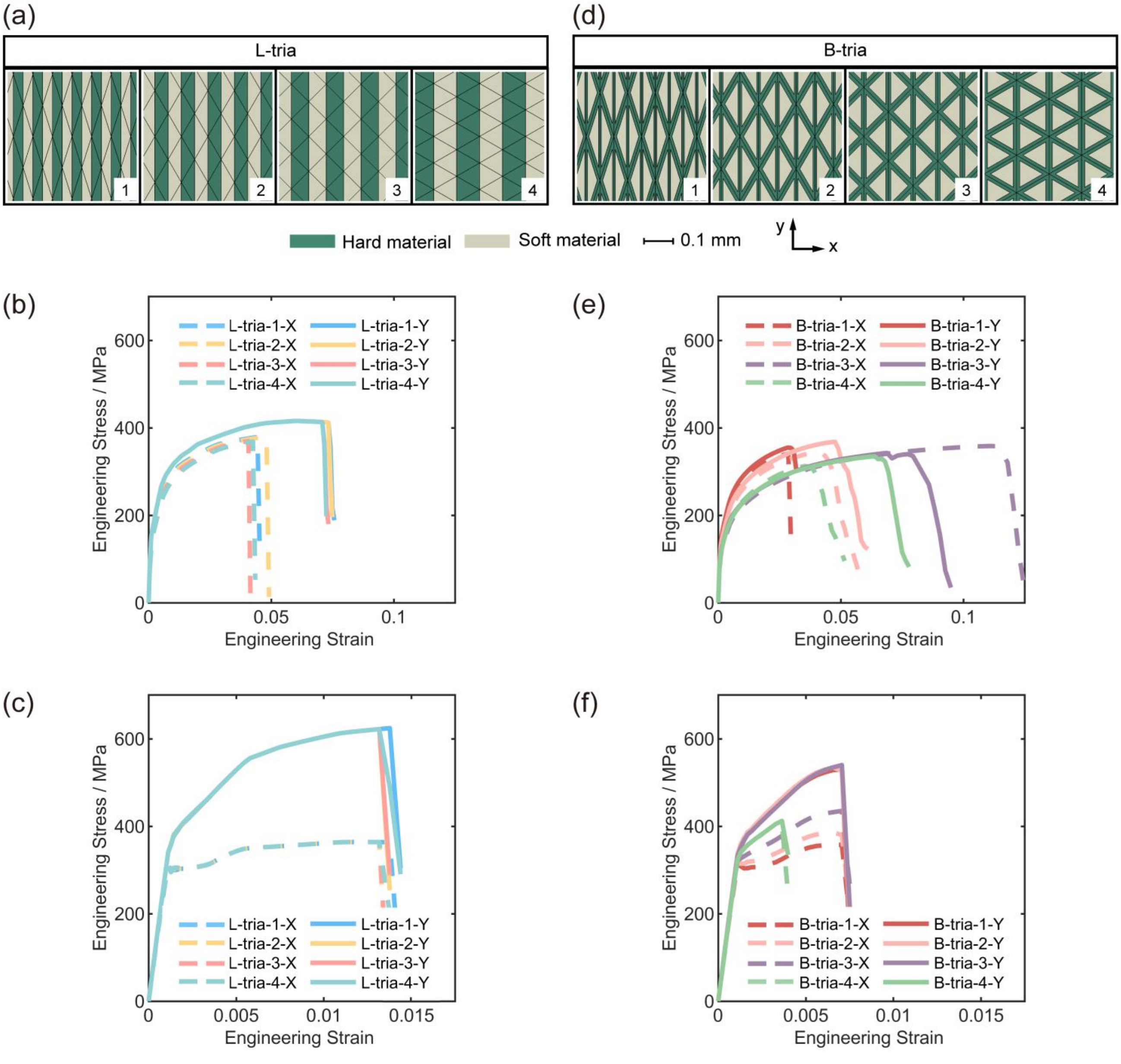


Fig. A1 Schematic diagrams of the triangular tessellation composites and the engineering stress-strain curves. Laminated structures: (a) Schematic diagrams of the models; (b) Uniaxial tension stress-strain curves; (c) Biaxial tension stress-strain curves. Brick-mortar structures: (d) Schematic diagrams of the models; (e) Uniaxial tension stress-strain curves; (f) Biaxial tension stress-strain curves.

Schematic diagrams of the laminated and brick-mortar models of the triangular tessellation composites and their stress-strain curves are shown in Fig.A1. Comparing the uniaxial tensile results of the two configurations (Fig. A1 (b), Fig. A1 (e)), it is clearly that the laminated structures exhibit greater strength when subjected to tension along the hard-phase compared to the X-axis direction. Conversely, the brick-mortar structures demonstrate comparable tensile behavior in both directions. Notably, the plasticity of the brick-mortar model scheme B-tria-3 in the X-direction is nearly twice as high as that of the laminated model. In the case of biaxial tension, the laminated structures demonstrate superior strength and plasticity compared to the brick-mortar structures.

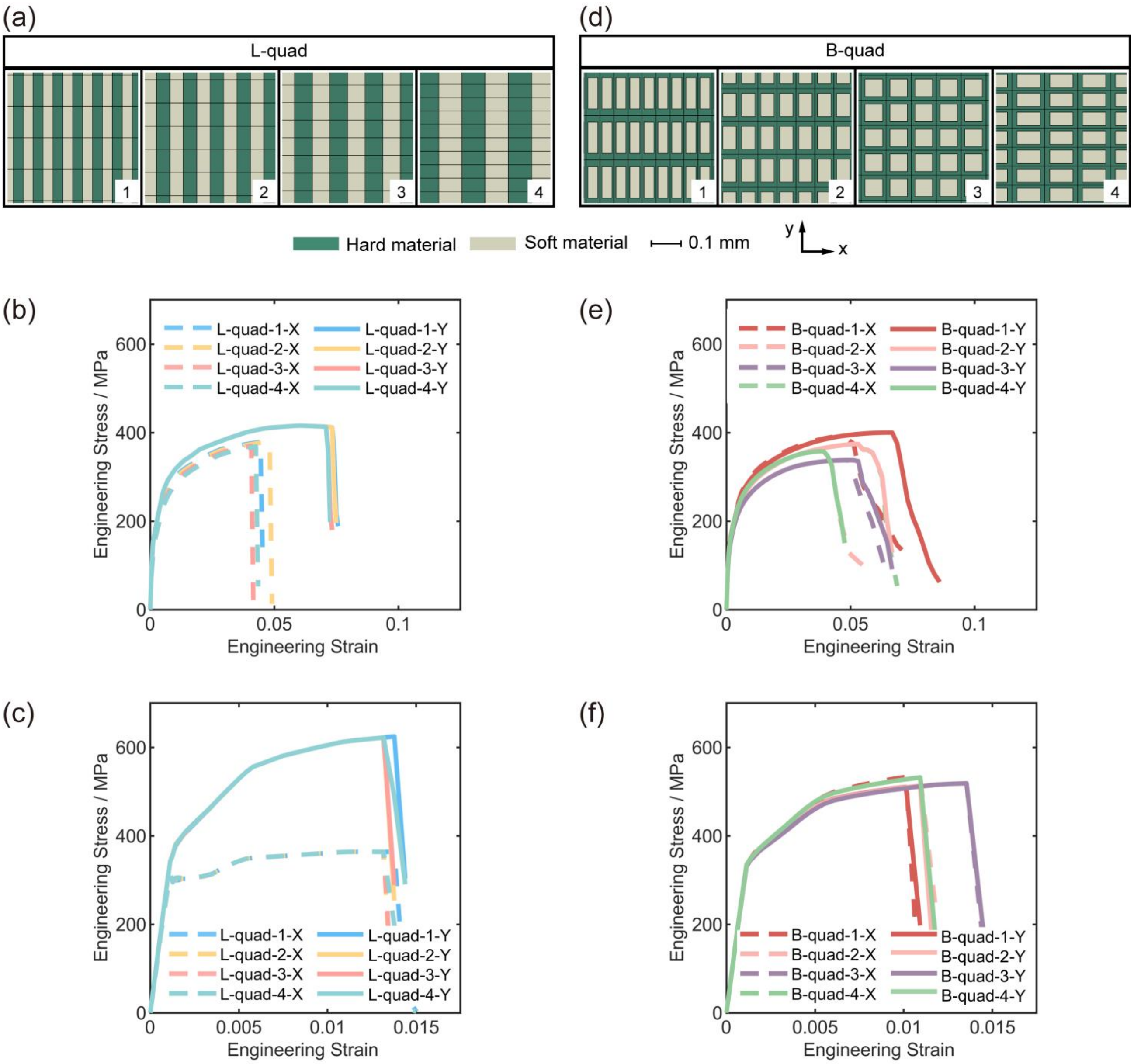


Fig. A2 Schematic diagrams of the quadrangular tessellation composites and the engineering stress-strain curves .

Laminated structures: (a) Schematic diagrams of the models; (b) Uniaxial tension stress-strain curves; (c) Biaxial tension stress-strain curves. Brick-mortar structures: (d) Schematic diagrams of the models; (e) Uniaxial tension stress-strain curves; (f) Biaxial tension stress-strain curves.

Schematic diagrams illustrating the laminated and brick-mortar models of the quadrangular tessellation composites, along with their corresponding stress-strain curves, are presented in Fig. A2. The stretching behavior of the laminated models of the quadrangular tessellation remains consistent with that of the triangular tessellation, as interfacial effects are not considered. Additionally, the strength and plasticity are comparable to those of the laminated structures because the brick-mortar structures primarily undergo stretching-dominated deformation. Furthermore, the anisotropic behavior of the brick-mortar models of the quadrangular tessellation is not particularly pronounced under isobiaxial stretching conditions.

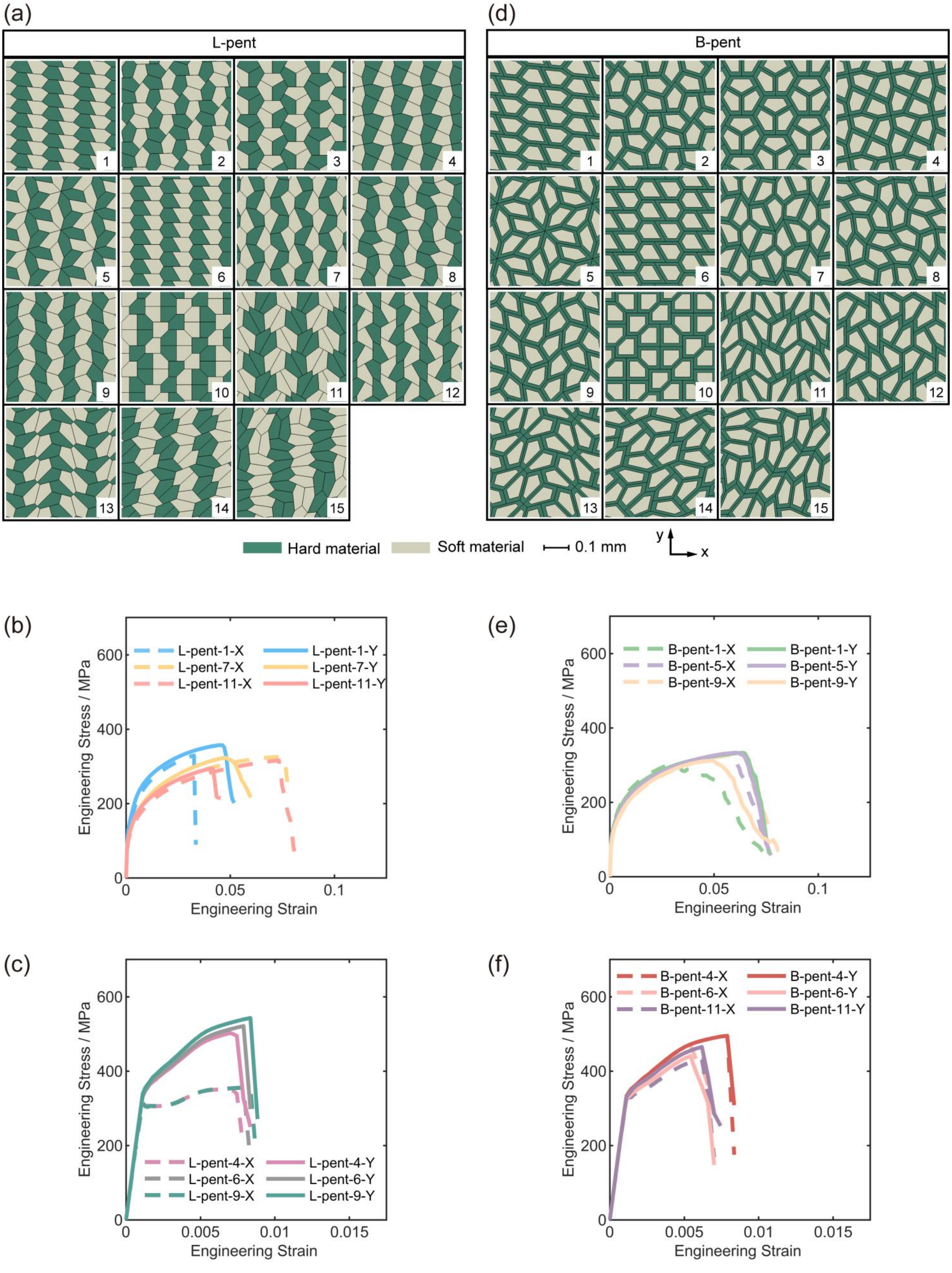


Fig. A3 Schematic diagrams of the pentagonal tessellation composites and the engineering stress-strain curves. Laminated structures: (a) Schematic diagrams of the models; (b) Uniaxial tension stress-strain curves; (c) Biaxial tension stress-strain curves. Brick-mortar structures: (d) Schematic diagrams of the models; (e) Uniaxial tension stress-strain curves; (f) Biaxial tension stress-strain curves.

The schematic diagrams of laminated and brick-mortar models of the pentagonal tessellation and their stress-strain curves are shown in Fig. A3. Due to the abundance of data, only the schemes demonstrating superior strength and plasticity performances have been selected for presentation. However, the strain localization issue associated with their sharper geometrical patterns leads to reduced material plasticity in both configurations.

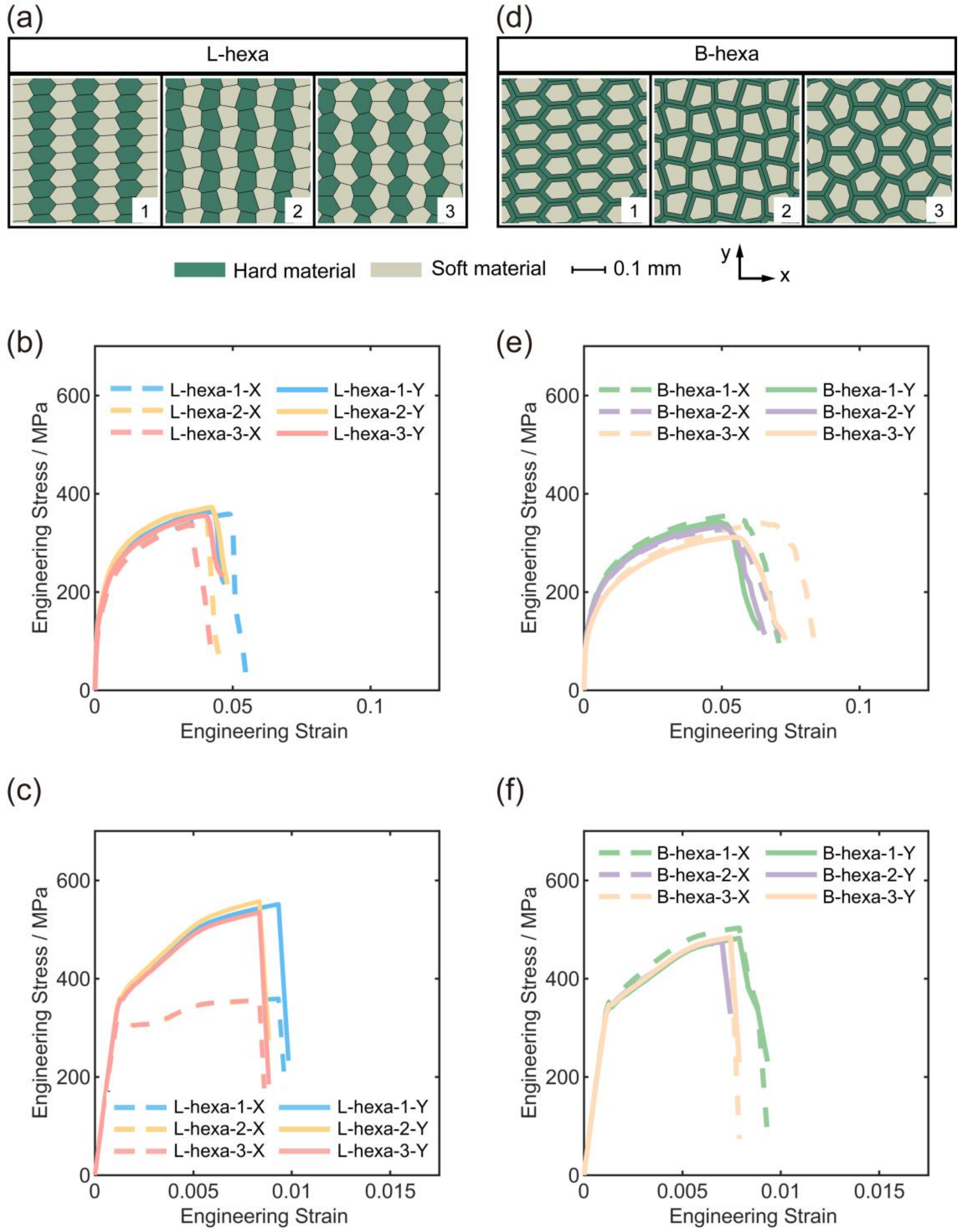


Fig. A4 Schematic diagrams of the hexagonal tessellation composites and the engineering stress-strain curves.

Laminated structures: (a) Schematic diagrams of the models; (b) Uniaxial tension stress-strain curves; (c) Biaxial tension stress-strain curves. Brick-mortar structures: (d) Schematic diagrams of the models; (e) Uniaxial tension stress-strain curves; (f) Biaxial tension stress-strain curves.

The schematic diagrams of laminated and brick-mortar models of the hexagonal tessellation and their stress-strain curves are depicted in Fig. A4. Similar to the pentagonal tessellation schemes, the reduced plasticity observed in these tessellation schemes can be attributed to the strain localization issue associated with their geometrical patterns.

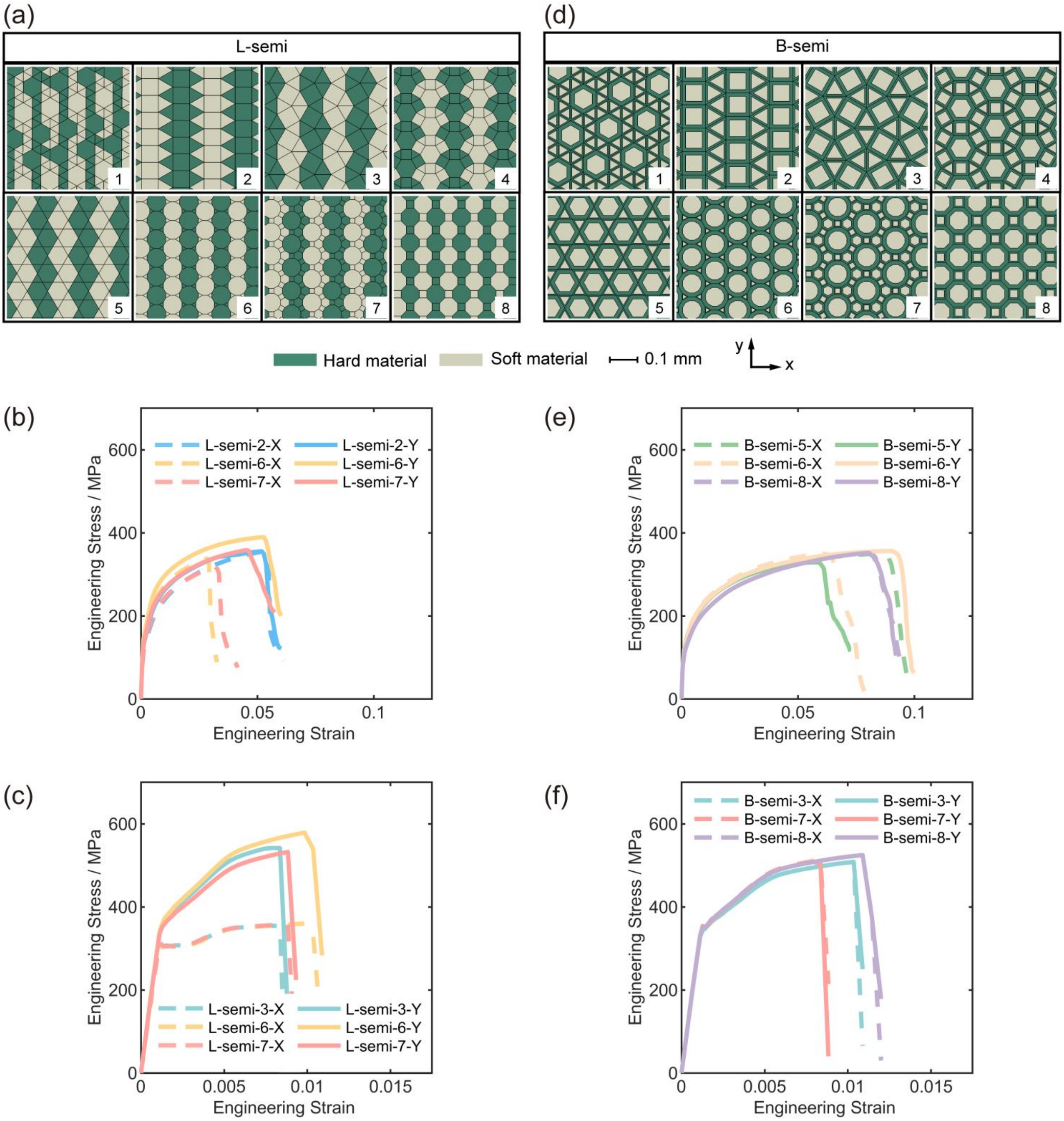

Fig. A5 Schematic diagrams of the semi-regular tessellation composites and the engineering stress-strain curves. Laminated structures: (a) Schematic diagrams of the models; (b) Uniaxial tension stress-strain curves; (c) Biaxial tension stress-strain curves. Brick-mortar structures: (d) Schematic diagrams of the models; (e) Uniaxial tension stress-strain curves; (f) Biaxial tension stress-strain curves.

Schematic diagrams of the laminated and brick-mortar models of the semi-regular tessellation and their stress-strain curves are illustrated in Fig. A5. Notably, the brick-mortar models exhibit a combination of tensile and bending deformations, resulting in superior plasticity compared to the laminated structures.

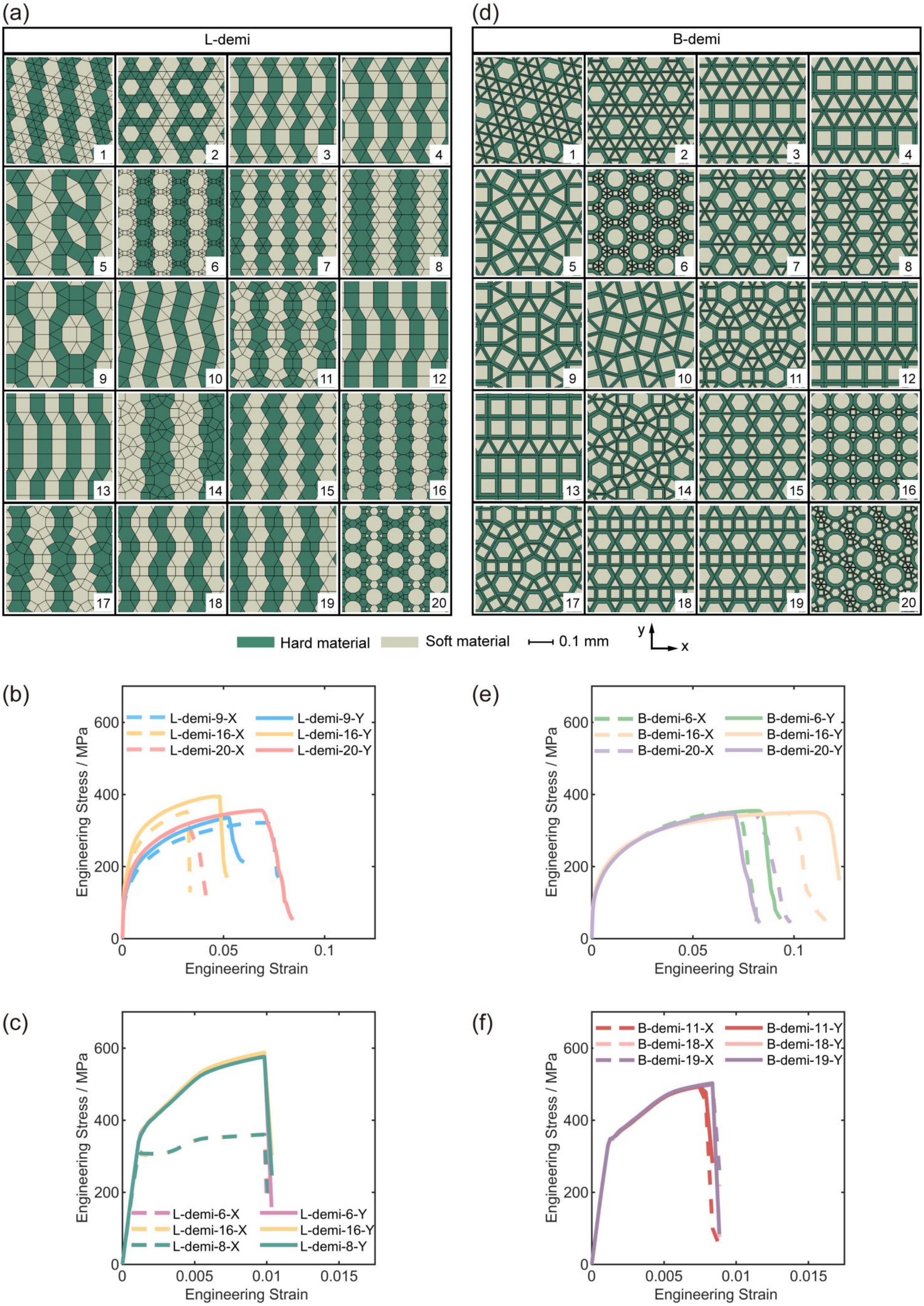

(a)
L-demi
(d)
B-demi
Hard material
Soft material
0.1 mm
y
x
(b)
L-demi-9-X
L-demi-9-Y
L-demi-16-X
L-demi-16-Y
L-demi-20-X
L-demi-20-Y
Engineering Stress / MPa
Engineering Strain
(e)
B-demi-6-X
B-demi-6-Y
B-demi-16-X
B-demi-16-Y
B-demi-20-X
B-demi-20-Y
(c)
L-demi-6-X
L-demi-6-Y
L-demi-16-X
L-demi-16-Y
L-demi-8-X
L-demi-8-Y
(f)
B-demi-11-X
B-demi-11-Y
B-demi-18-X
B-demi-18-Y
B-demi-19-X
B-demi-19-Y

Fig. A6 Schematic diagrams of the demi-regular tessellation composites and the engineering stress-strain curves. Laminated structures: (a) Schematic diagrams of the models; (b) Uniaxial tension stress-strain curves; (c) Biaxial tension stress-strain curves. Brick-mortar structures: (d) Schematic diagrams of the models; (e) Uniaxial tension stress-strain curves; (f) Biaxial tension stress-strain curves.

Schematic diagrams of the laminated and brick-mortar models of the demi-regular tessellation and their stress-strain curves are shown in Fig. A6. Similar to the semi-regular tessellation models, the brick-mortar models exhibit a combination of stretching and bending deformations, resulting in higher plasticity compared to the laminated structures.

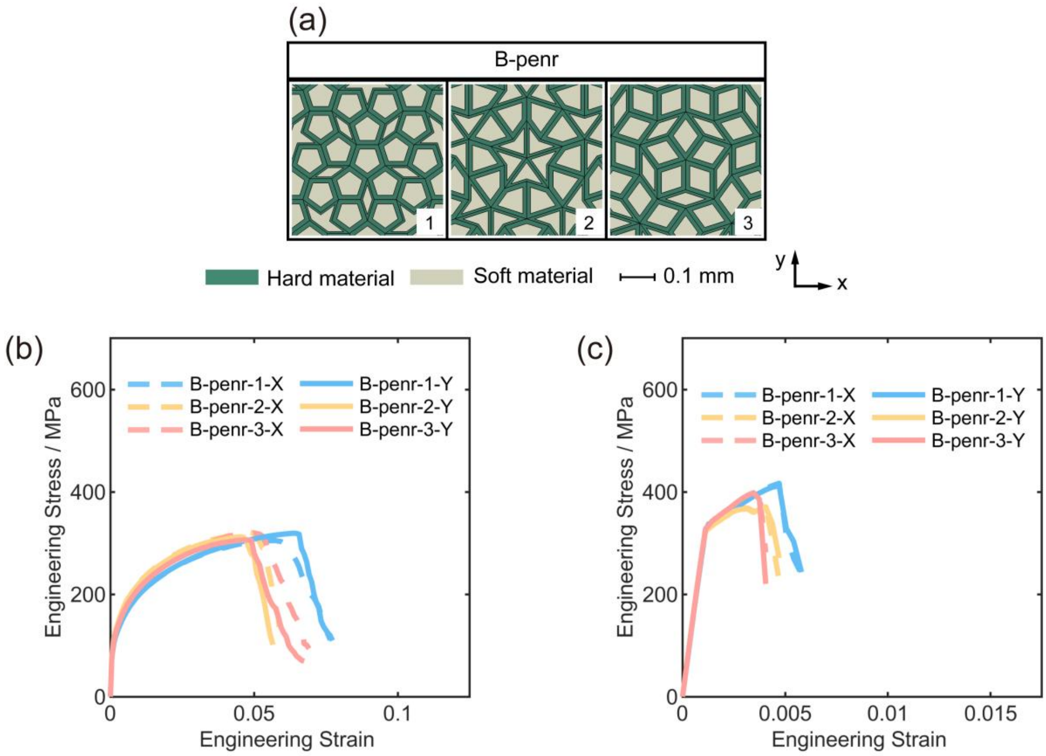


Fig. A7 Schematic diagrams of brick-mortar structures of the Penrose aperiodic tessellation and the engineering stress-strain curves: (a) Schematic diagrams of the models; (b) Uniaxial tension stress-strain curves; (c) Biaxial tension stress-strain curves.

Schematic diagrams of the brick-mortar models of the Penrose aperiodic tessellation and their stress-strain curves are illustrated in Fig. A7. The material primarily experiences bending deformation, and its intricate geometry contributes to heightened susceptibility to strain localization, simultaneously resulting in diminished strength and plasticity of the material.

In section 2.2, we employ the inverse finite element method to calibrate the parameters of the

GTN constitutive model. The engineering stress-strain curves obtained from experiments and numerical simulations are illustrated in Fig. A8.

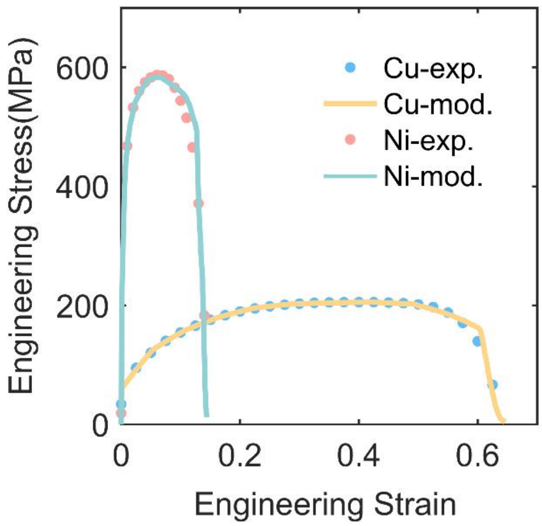


Fig. A8 Comparison of experimental and numerical simulation results for uniaxial tensile testing of copper and nickel.